



Scanning electron microscopy cathodoluminescence of quartz: Principles, techniques and applications in ore geology



Stefanie N. Frelinger, Matthew D. Ledvina, J. Richard Kyle, Donggao Zhao *

Department of Geological Sciences, Jackson School of Geosciences, University of Texas at Austin, Austin, TX 78712, USA

ARTICLE INFO

Article history:

Received 1 April 2014

Received in revised form 1 October 2014

Accepted 8 October 2014

Available online 29 October 2014

Keywords:

Scanning electron microscopy

Cathodoluminescence

Hydrothermal quartz

Porphyry deposits

ABSTRACT

Scanning electron microscopy cathodoluminescence (SEM-CL) of quartz has been a prevalent research technique in porphyry and epithermal systems for the past two decades. Quartz from specific geological environments reveals unique textures in SEM-CL, which can be used to constrain the evolution of these ore-bearing systems when complemented by fluid inclusion, hyperspectral mapping, and trace element studies. We review SEM-CL principles and instrumentation, sample preparation and handling, and experimental conditions of quartz SEM-CL imaging that result in the high quality CL images. The effects of sample polishing, accelerating voltage, beam spot size, working distance, vacuum conditions, image acquisition, and post-processing were examined through experimental trial. For the XL 30 ESEM and the attached Gatan PanaCL detector used, the optimum experimental conditions to obtain high quality panochromatic SEM-CL images of quartz at high vacuum mode for carbon-coated conductive samples are as follows: 15 kV accelerating voltage, relative beam spot size 6 (approximately 500 nm in diameter), HT – 570 V to – 580 V photomultiplier tube (PMT) voltage. Low vacuum mode (with chamber H₂O vapor pressure from 0.1 to 1.0 Torr) working conditions are similar to the conditions at high vacuum mode except the PMT voltage should be reduced to – 550 V to – 560 V. Working distances vary based on the position of user's retractable CL detector. The sample surface should be as close as possible to the CL detector, but a 1 mm clearance between the detector and the sample surface is recommended to prevent detector from possible damage by the sample. Several minutes of beam exposure prior to image acquisition at 320 second scan speeds at 50×–1500× magnifications is recommended to generate the greatest CL emission. Monochromatic CL imaging requires three scans over the same area using red, green, and blue optical filters that can be merged to produce a "true color" image. The red and green filters require stronger PMT voltages to produce sufficient CL emissions by an increase of – 200 V to – 300 V and – 150 V to – 200 V, respectively, from the PMT voltage used for panochromatic imaging. Special attention is given to the challenges associated with imaging hydrothermal quartz veining in ore deposits and the value of CL data as a foundation for geochemical studies. SEM-CL imaging of vein quartz is explored through case studies of the Red Hills Porphyry Cu–Mo Deposit, Texas, USA, and the Ertsberg–Grasberg Cu–Au District, Papua, Indonesia to aid in vein paragenesis. The most common application of quartz SEM-CL in ore geology is to reveal the relative timing of mineral precipitation, mineral dissolution, and inherited structural features. Understanding of temporal relations among these events makes it possible to select specific generations of quartz within a vein for further studies such as the TitaniQ thermometry and fluid inclusion microthermometry in order to establish T–P–X fluctuations throughout the development of a hydrothermal system.

© 2014 Elsevier B.V. All rights reserved.

1. Introduction

When an electron beam bombards a sample in a scanning electron microscope (SEM) or electron probe microanalyzer (EPMA), many signals, such as secondary electron (SE), backscattered electron (BSE),

characteristic X-ray, visible light, etc., are produced. Crookes (1879) first observed the phenomenon of cathodoluminescence (CL), the emission of light by high energy electron bombardment of a mineral, in the 1870s. Since Crookes' observation, CL has been used in numerous petrologic studies of quartz from a variety of geologic environments (Seyedolali et al., 1997), particularly in sedimentary rocks and hydrothermal ore deposits, because CL can illuminate textures which are not observable by other methods (transmitted light, SE, BSE, etc.). Common minerals utilized for CL petrography include quartz, zircon, diamond, corundum, apatite, anhydrite, fluorite, carbonates, etc. (e.g., Götze et al., 2001; Machel and Burton, 1991; Pagel et al., 2000).

* Corresponding author at: Department of Geological Sciences, Jackson School of Geosciences, University of Texas at Austin, 2275 Speedway Stop C9000, Austin, TX 78712, USA. Tel.: +1 512 471 1177.

E-mail address: dzhao@utexas.edu (D. Zhao).

The geologic applications of quartz CL include crystal growth, dissolution, replacement, deformation, and provenance (Boggs et al., 2002; Landtwing and Pettke, 2005; Matter and Ramseyer, 1985; Penniston-Dorland, 2001; Rusk, 2012; Rusk and Reed, 2002; Seyedolali et al., 1997). In sedimentary petrography, Sippel (1968) used CL to determine texture, sediment source, degree of compaction, diagenetic history, ratio of authigenic and detrital minerals, stratigraphy, siliciclastic components, and cementation history in quartz sandstones. Owen and Carozzi (1986) also deduced stratigraphy, siliciclastic components, and cementation history of the Jackfork Sandstone, Arkansas. Studies using CL by Müller et al. (2003a) in conjunction with trace element variations in igneous quartz were used to correlate CL zoning patterns with genetic processes such as magma mixing, velocity of ascent, growth and diffusion rates of the melt, and large scale convection within a magma chamber. Metamorphic petrography by Spear and Wark (2009) also used CL fabrics of plastically deformed quartz for Titanium thermometry, whereas Sprunt (1978) determined that the luminescence color of metamorphic quartz can be correlated with metamorphic grade (red: low temperature, blue: high temperature) in addition to deformation mechanisms by mechanically induced defects.

Early studies of quartz CL examined the color variations using optical-CL by either cold- or hot-cathode systems (Marshall, 1988; Matter and Ramseyer, 1985; Seyedolali et al., 1997; Zinkernagle, 1978). The major disadvantages of this instrumentation include low magnifications and resolution of images partly due to the detectors inability to detect CL emissions outside the visible range of the electromagnetic spectrum. Provenance studies were limited by the efficacy of optical-CL until the advent of attaching a CL detector to an SEM. This SEM-CL technique made more detailed CL imaging possible due to higher resolution and magnification capabilities which greatly improved observations of distinct CL textures. The intensity of SEM-CL emissions is dependent on the geochemical and structural variations within a crystal which makes this technique ideal for examining textural, compositional, and structural information for any given sample.

The application of quartz SEM-CL has been a robust research technique used in hydrothermal ore systems for the past two decades (Götze et al., 2011; Lehmann et al., 2009; Marshall, 1988; Rusk, 2012; Rusk and Reed, 2002; Rusk et al., 2008a,b; Vasyukova et al., 2013a,b). When various quartz generations and their textural variations within a single, potentially ore-bearing vein are recognized by CL, a preliminary interpretation of quartz growth histories related to ore deposition can be constructed. CL patterns can then be used in conjunction with fluid inclusion microthermometry, trace element compositional variation, and isotopic compositional analyses to relate to specific mineralization events (Donovan et al., 2011; Flem et al., 2002; Götze et al., 2011; Landtwing and Pettke, 2005; Leeman et al., 2012; Müller et al., 2003a, b; Rusk, 2012; Rusk et al., 2008a,b). Therefore, it is imperative to capture high quality CL images during the initial research phase of vein quartz for proper follow-up analyses.

The goal of this review is to provide a general outline of the SEM-CL principles and optimal experimental conditions to capture high quality SEM-CL images and to apply the SEM-CL technique to quartz derived from epithermal and porphyry environments. The authors recognize that obtaining quality SEM-CL images is dependent largely on samples, sample preparation and experimental conditions specific to the instrument used. Case studies of the Red Hills porphyry Mo–Cu, Texas, and the Ertsberg–Grasberg porphyry–skarn Cu–Au, Indonesia deposits utilizing these SEM-CL techniques are used to illustrate the application of SEM-CL for ore geology research.

2. Principles and instrumentation of SEM-CL

SEM-CL is a near surface effect, that can be used to reveal complex crystal growth histories and cryptic microtextures of luminescing minerals which are otherwise invisible with optical, SE, and BSE imaging (Marshall, 1988). When an electron beam is scanned across

the polished surface of a sample, the CL signal is captured by a parabolic or elliptical mirror and a digital CL image is produced as visible light is incident upon the surface of the photomultiplier.

According to Marshall (1988), Boggs et al. (2002), Götze (2009), Götze and Freiberg (2012), and Henry (2012), this technique can be explained by the solid state band theory in which a high energy electron beam bombards a material causing the excitation of electrons to move from the low energy valence band toward the higher energy conduction band. Once the electron reaches the conduction band and the transient energy begins to diminish, the electron will travel back to the valence band and return to ground state energy. When returned to ground state energy, a small amount of radiation (light) is released and translated into wavelengths in the visible light (400–700 nm) or ultra violet light (>400 nm) spectrum. This emission of light is captured via a photomultiplier tube and used to construct an image of the samples luminescence (Fig. 1).

The space between the valence and conduction bands that the electron must pass through is known as the band gap. The band gap may contain holes or traps caused by intrinsic or extrinsic defects in the material which may capture the electrons momentarily. Once the electron is able to escape the trap and recombine in the valence band, a photon is emitted and luminescence will also occur (Fig. 1c).

3. Causes and textures of quartz SEM-CL

Quartz derived from plutonic, volcanic, metamorphic, and hydrothermal systems emit unique CL signatures that can aid in identifying different generations of quartz formed in a specific geologic environment. The reader is referred to Rusk (2012) for illustrations on the following quartz SEM-CL texture descriptions.

3.1. Causes of quartz SEM-CL

Luminescence intensity is dependent on the density of intrinsic and extrinsic defects within the band gap. Intrinsic defects are structural imperfections in the quartz crystal due to vacancies within the crystal lattice. The most common types are point defects, translations, radiation damage, shock damage, melt inclusions, and fluid inclusions which reflect the actual structure of the crystal and may ultimately provide information of the physiochemical conditions during mineralization and subsequent post-mineralization events such as deformation or metamorphism. Fig. 2 displays a quartz SEM-CL image taken by Baline (2007) of hydrothermal quartz from the early Kali stockwork of the Ertsberg–Grasberg district where a bright-CL zone is caused by the abundance of fluid inclusions trapped during a specific period of crystal growth. Therefore, the intrinsic defects can reflect the genetic processes of crystal growth and the specific physiochemical conditions following afterwards (Hamers and Drury, 2011; Müller et al., 2003b; van den Kerkhof et al., 2004).

Extrinsic defects include impurities of cations and anions that have been substituted into the crystal structure. These impurities can be cathodoluminescence activators, sensitizers, and quenchers which are mineral specific. Trace element concentrations and their relative proportion to one another in quartz are considered the major proponents that influence the CL response in most luminescent minerals (Götze et al., 2001; Müller et al., 2003b; Pagel et al., 2000). Quartz's high purity only allows a limited number of trace elements such as Ti^{4+} , P^{5+} and Ge^{4+} to substitute for Si^{4+} within the crystal lattice. Trivalent cations such as Al^{3+} , Ga^{3+} , and Fe^{3+} coupled with H^+ , Li^+ , Na^+ and K^+ monovalent cations for charge balance may also substitute for Si^{4+} (Bahadur, 1993; Dennen, 1965; Lehmann, 1975; Müller et al., 2003a; Weil, 1984). Baline (2007) correlated bright-CL growth zones with elevated concentrations of Ti^{4+} and Al^{3+} from Kali stockwork hydrothermal quartz from the Ertsberg–Grasberg district (Fig. 3). As the CL bright and dark zones are largely deposit specific and the relations between CL zonations and abundances of trace elements in quartz are uncertain,

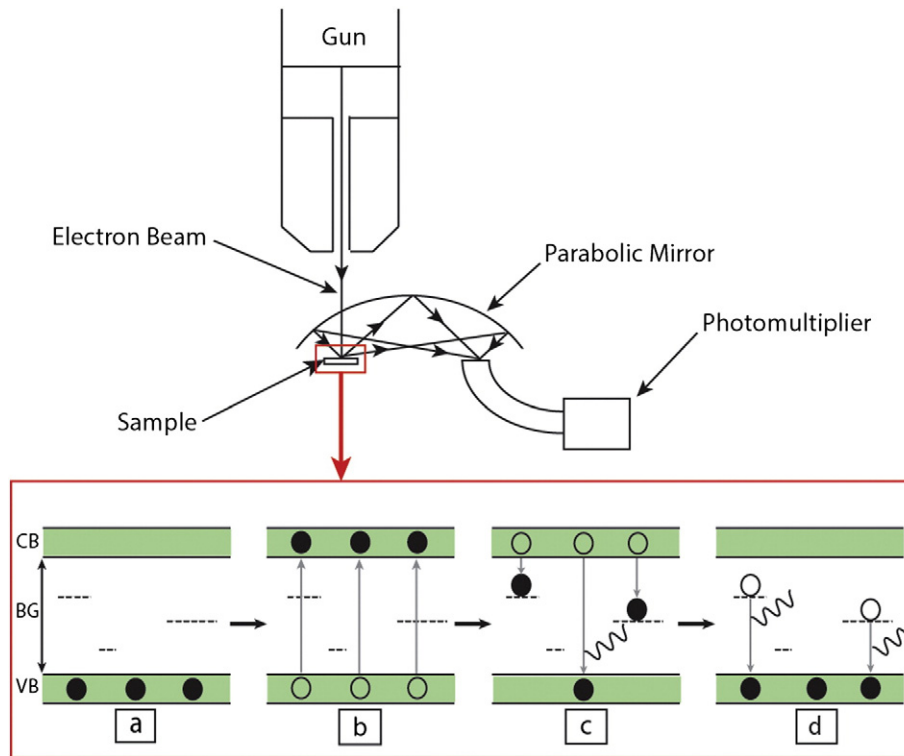


Fig. 1. SEM-CL explained by the solid state band theory. Filled circles represent electrons at the location specified in the energy levels at stages a, b, c, and d while unfilled circles represent the prior location of the previous energy stage. a) Unexcited electrons compartmentalized in the valence band at ground state energy, b) electrons excited by electron beam bombardment transition from the valence band to conduction band, c) as the energy diminishes, the electrons will retreat back to the valence band and emit luminescence unless a trap falls within the electron's path, and d) electrons will overcome the barrier trap and return to the valence band causing further luminescence (Modified from Boggs et al., 2002 and Henry, 2012).

interpretations of CL caused by trace element concentration should be handled on a case by case basis.

Activators of CL signals in quartz include Ti in quartz in high temperature (>400 °C) porphyry environments and Al in quartz in low

temperature (<300 °C) epithermal environments. Rusk et al. (2008b) showed positive correlations of compositional zonations of Ti with highly luminescent quartz in the Butte porphyry Cu system. In contrast, Baline (2007) was not able to correlate Ti concentration with all CL textural zonations, but was able to detect Ti in 7 of 11 trace element maps. Iron, Ge, P, Sb, K, and Li have also been reported to act as CL activators or quenchers in quartz, but currently no systematic relationships have been reported. Rusk et al. (2008b) also showed that Al negatively correlated with luminescence intensities in quartz from the Butte porphyry Cu deposit. They proposed that the fluctuations in Al represent the changes in pH of the hydrothermal fluids and the rates of quartz precipitation. Baline (2007) showed late stage, dark CL quartz from the Grasberg-Ertsberg district contain elevated levels of Fe compared to bright CL quartz which suggests Fe suppresses CL response. Hyperspectral mapping of CL emission bands in hydrothermal quartz by Götte et al. (2011) showed that elevated Li^+ and H^+ cation concentrations represent periods of rapid precipitation in hydrothermal quartz crystals from Gigerwald, Switzerland and Rohdenhaus, West Germany.

3.2. Textures of quartz SEM-CL

3.2.1. Plutonic quartz

Plutonic quartz typically emits dark CL cores with bright rims and may also exhibit dark CL microfractures, dissolution, or recrystallization textures (Müller et al., 2003). CL intensities of growth zones are usually weak to nonexistent. Oscillatory growth zones typically mimic embayment outlines of partially dissolved precursor quartz and groundmass quartz emit homogenous, bright CL (Müller et al., 2002). Scanning magmatic quartz using red, green, and blue (RGB) monochromatic filters typically reveals magmatic quartz to luminesce red to violet (Zinkernagle, 1978).

SEM-CL imaging of growth and dissolution features of quartz eyes found in porphyry environments by Vasyukova et al. (2013a,b) records

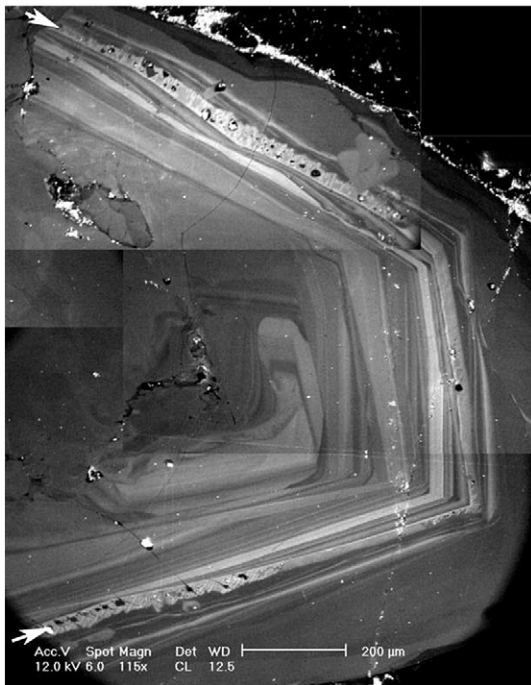


Fig. 2. Composite image of a bright luminescent zone containing abundant primary fluid inclusions in quartz in the early Kali stockwork, Ertsberg–Grasberg District, Indonesia. White arrows point to the zone of fluid inclusions which emit a bright-CL growth zone. From Baline (2007).

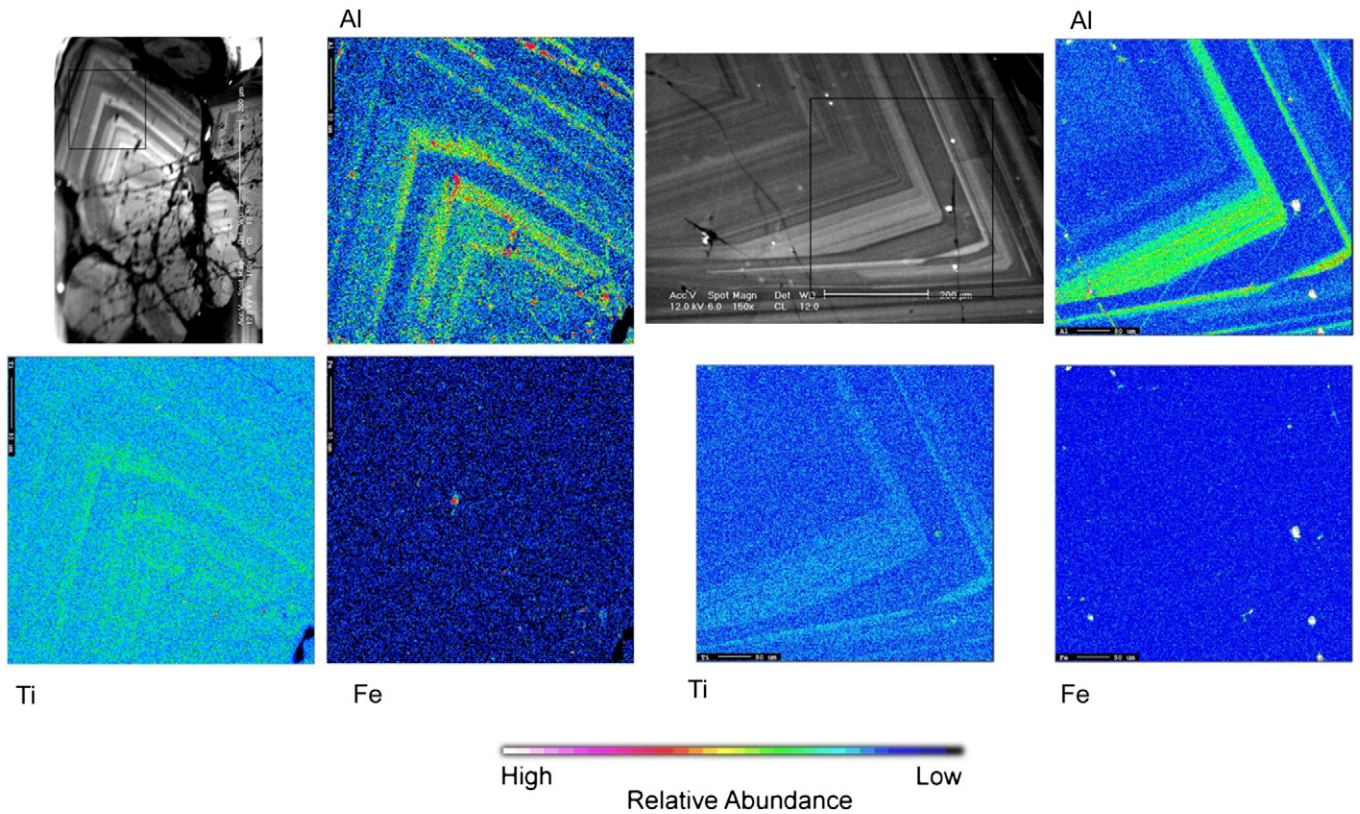


Fig. 3. Al, Ti, and Fe trace element maps of well-zoned quartz from the Dalam Diorite stockwork, Ertsberg–Grasberg District, Indonesia. Al and Ti positively correlate with bright CL zones while Fe displays no correlation with CL zones. From Baline (2007).

post-magmatic cyclicality of quartz crystallization, pressure buildup, fluid exsolution, and continuous cooling under non equilibrium conditions throughout the life span of a porphyry system. Bernet and Bassett (2005) attribute the formation of post-magmatic microcracks to the variation of thermal stresses from cooling of the magma.

3.2.2. Volcanic quartz

Volcanic quartz phenocrysts typically show well preserved growth zones of oscillating CL intensities. Periods of crystal growth, re-adsorption, and subsequent growth again cause volcanic quartz to become more rounded and embayed (Bernet and Bassett, 2005). Zinkernagle (1978) and Marshall (1988) reported volcanic quartz will emit red to violet luminescence similar to plutonic quartz.

3.2.3. Metamorphic quartz

Metamorphic quartz typically emits a dull and homogenous CL response (Rusk, 2012). This texture has been suggested to represent annealing of the quartz grain by recrystallization or polygonization, which effectively increases the crystal order, reducing the number of structural defects in the crystal and purifying the crystal by the removal of impurities thus producing a homogenous CL response (Boggs et al., 2002). Recrystallized quartz by grain boundary migration described by Van den Kerkhof et al. (2004) emit lower CL along the rims of the grain which correlate with zones rich in fluid inclusions. Spear and Wark (2009) report a general increase in CL intensity with metamorphic grade and a wide range of quartz CL textures in pelitic schist, which are attributed to crystallization, recrystallization, reprecipitation from fluids, strain release, and diffusion. Rusk (2012) reported that quartz in orogenic Au deposits typically generates a dull gray, homogenous CL response and mottled textures for panochromatic images. Monochromatic images of metamorphic quartz will emit brown luminescence (Zinkernagle, 1978).

3.2.4. Hydrothermal quartz

In comparison to volcanic, plutonic, or metamorphic quartz, hydrothermal quartz displays the greatest range of CL textures. Hydrothermal quartz textures illuminated by SEM-CL include precipitation–dissolution textures and microfractures which are representative of large scale physiochemical changes within the hydrothermal system (Rusk et al., 2008a,b). Zinkernagle (1978) reported blue to violet CL emission using RGB monochromatic filters, which is typical for hydrothermal quartz (Fig. 4). The reader is referred to additional figures in Rusk (2012) that illustrate the variety of CL patterns specific to epithermal and porphyry systems.

4. Sample preparation, experimental conditions and image processing

In general, the electron beam is rastered across a large area of the sample and the CL response is recorded with digital images from the CL detector. The CL images can be obtained over a range of magnifications (10 to 10,000×), but the lowest magnification is constrained by the specific configuration of the SEM and attached CL detector system. The image acquisition procedure varies depending on the information that is sought.

4.1. Sample preparation

SEM-CL imaging requires a flat, well-polished (preferably doubly polished) thin or thick section. Polishing is a key limitation to procure a quality CL image so additional polishing by a vibratory polisher with colloidal silica on the order of 3–8 h is recommended, depending on the existing polish state and the desired mineral to be imaged. Extended polishing of softer minerals should be avoided to prevent the polisher from grinding away portions of the section.

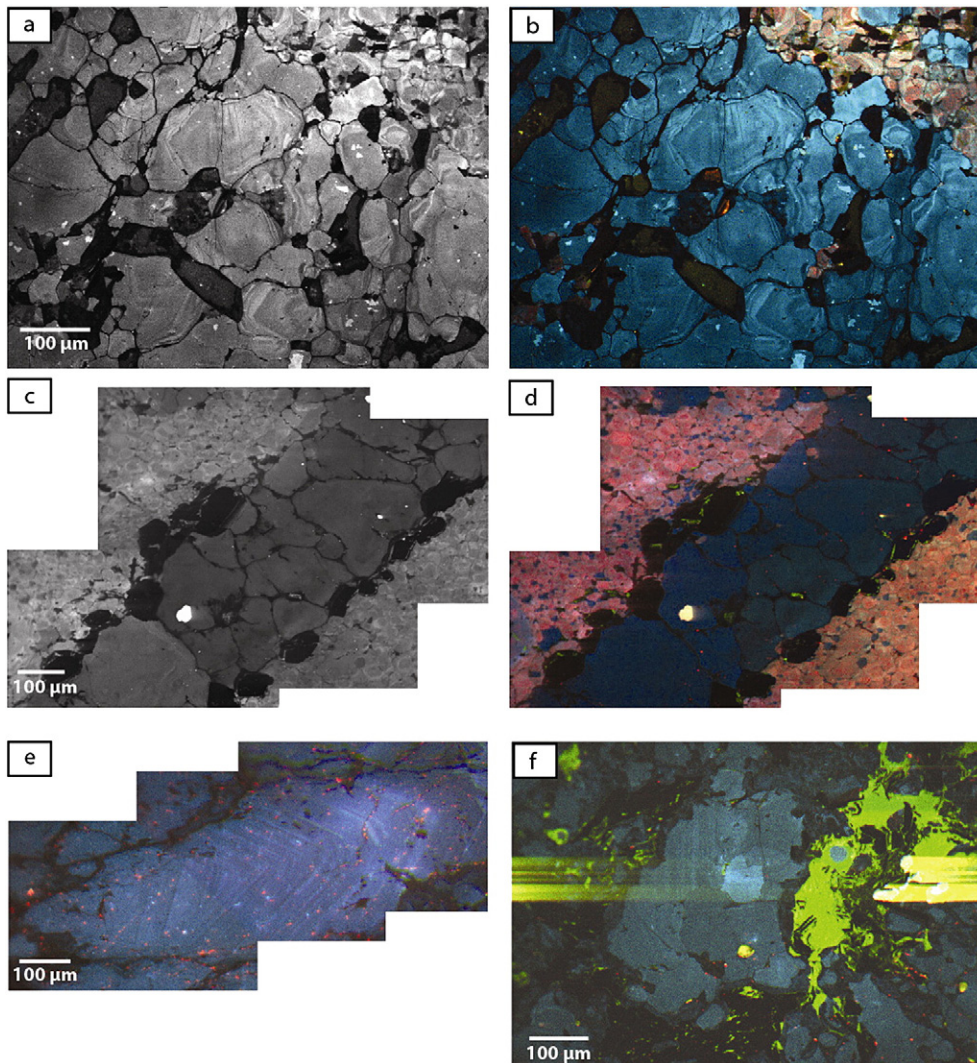


Fig. 4. Merged RGB SEM-CL images of the Red Hills porphyry Mo–Cu deposit. a–b) panchromatic (a) and monochromatic (b) of an early stage, barren blue luminescent hydrothermal quartz veins and red luminescent ground mass quartz. c–d) panchromatic homogenous gray scale CL (c) and monochromatic (d) image of a blue luminescent, lower temperature quartz-pyrite vein embedded in red luminescent quartz groundmass. e) Monochromatic images of a euhedral, hydrothermal quartz crystal with red luminescent inclusions. f) Monochromatic image of hydrothermal quartz of 3 generations, each displaying variable blue CL intensity surrounded by sericite and anhydrite groundmass. Images acquired at 12.0 mm working distance, 6.0 spot size, and 12 kV.

Highly luminescent minerals such as anhydrite and carbonates may be removed prior to section preparation to allow for maximum results for quartz imaging. These minerals are sensitive to degradation by prolonged exposure to the scanning electron beam and will overwhelm the CL detector when imaging quartz in high contrast settings. As a result, streaking or smearing will occur which adversely affects the quartz CL image as seen in Figs. 5 and 4f. Coating the sample with a 25–30 nm thick layer of carbon (measured using color changes to blue on brass) is necessary for proper sample conductivity and to prevent charging while at high vacuum conditions.

4.2. Sample degradation by SEM-CL

Experimental conditions (accelerating voltage, spot size, etc.) and length of exposure to the beam may influence the localized thermal effect of the beam on the sample surface. If subsequent fluid inclusion microthermometry or trace element studies are anticipated following SEM-CL imaging, certain precautions must be taken.

Xu (2012) reported panchromatic SEM-CL imaging of quartz grains in thick sections produced no ill net effects for later fluid inclusion microthermometry work. Monochromatic SEM-CL imaging, however, requires longer beam exposure times and higher PMT voltages which

may induce minor damage on the sample. Near surface fluid inclusions at 5–10 μm depth in 100 μm thick sections became decrepitated for low temperature (80–200 °C) quartz grains, but inclusions located at a depth greater than 10 μm in thick sections were not affected. Landtwing and Thomas (2005) also conducted fluid inclusion thermometry studies after completing CL imaging, and no difference was observed during the collection of homogenization temperature and salinity measurements. Removal of the first 10 μm of the sample should be completed before any fluid inclusion work is to be performed in order to adequately remove the carbon coat and any near surface fluid inclusions.

Trace element analyses of quartz by EPMA, SIMS, or LA-ICPMS can also be conducted on the same thick section sample used for CL imaging so long as 10 μm of the sample surface is removed. Diffusion of trace elements in highly resistive minerals such as quartz, zircon, and diamond is highly unlikely from the bombardment of electrons by SEM-CL. Risk of errant trace element values in quartz by these analytical methods is small particularly by LA-ICPMS because roughly 10–20 μm of the sample surface is ablated away (assuming a 45 s spot ablation time) which ensures a suitable penetration depth for the collection of trace element measurements. However, it is recommended that fluid inclusion and trace element studies should be completed on separate but

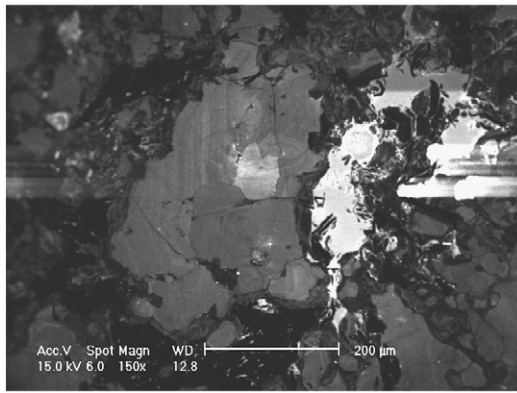


Fig. 5. SEM-CL image of hydrothermal quartz within dark-CL luminescent sericite matrix from the Red Hills porphyry Mo–Cu deposit, Texas shows white streaking caused by highly luminescent anhydrite. The presence of anhydrite degrades the quality of the SEM-CL image of quartz and should be removed prior to CL imaging.

identical sections from the same sample to eliminate any risk of fluid inclusion leakage or trace element migration caused by SEM-CL.

4.3. Experimental conditions

The authors recognize experimental conditions for SEM-CL varies according to the instrument and detector used by the researcher. The working conditions suggested below are the results of a combination of operation techniques found in the literature and personal experimentation using a Gatan PanaCL detector attached to the Philip/FEI XL30 ESEM in the Department of Geological Sciences at the University of Texas at Austin.

4.3.1. Beam spot size and accelerating voltage

A relative beam size 6 (approximately 500 nm in diameter) for the XL 30 ESEM is sufficient to produce a good SEM-CL image. In high vacuum modes with chamber pressures greater than 1 Torr, suitable accelerating voltages range from 12 to 15 kV. Figs. 6 and 7 compare panochromatic SEM-CL images of a hydrothermal quartz crystal taken with different accelerating voltages with the appropriate high tension photomultiplier tube voltages (PMT volts), brightness, and contrast adjustments: 7.5 kV, 12 kV, 15 kV, 20 kV, and 30 kV. The PMT volts

generally decrease by -30 V with each increment of increasing accelerating voltage. Lower accelerating voltages (7.5 kV) produce grainy images while higher accelerating voltages (20–30 kV) display foggy, diffuse boundaries of quartz growth zones. The 12 kV and 15 kV accelerating voltages produced the highest resolution images which reveal sharp growth zones. The CL intensities of growth zones are the clearest and display the highest contrast using 15 kV.

SEM-CL images obtained in low vacuum (0.1–1.0 Torr chamber pressure) typically have lower resolutions than those obtained in high vacuum mode. However if high vacuum settings are not used, working conditions with a 10–14 mm working distance, 5–6 beam spot size or probe diameter, and 15 kV accelerating voltage achieve the best images. Table 1 summarizes ideal PMT voltages based on the selected accelerating voltage at high vacuum and low vacuum modes for carbon-coated samples.

Proper working distances will vary based on the sample thickness and size of the users CL detector. The sample should be raised as close to the detector as possible, but far enough to avoid the risk of collision. A CCD camera within the instrument is useful to ensure proper clearance approximately 1–2 mm away from the detector.

4.3.2. Image focusing and CL detector centering

Prior to CL imaging, it is critical to focus the image in SE or BSE modes at a magnification that is three times higher than the anticipated magnification at which the CL image will be taken. CL images are routinely taken at 150 \times to 1500 \times magnification. The quality of an SEM-CL image will also be compromised if the CL parabolic mirror is not properly centered with the electron beam. Once the detector is inserted, use a low magnification and change the contrast and brightness until the outline of the hole on the parabolic mirror is visible. Adjust the detector appropriately until the hole is perfectly centered.

4.3.3. Beam exposure and scan speeds

Luminescence intensity is a time dependent process. To obtain higher contrast images, several minutes of beam exposure will enhance the CL emission (Xu, 2012). Similar to acquiring a high quality SE or BSE image, slow scan speeds are ideal to achieve the clearest panochromatic, gray scale image. Cathodoluminescence image quality is dependent on the intensity of quartz luminescence, the presence of other luminescent phases, sample preparation, and SEM settings. Resolution is highest where the intensity of quartz luminescence varies greatly. Regions where quartz luminescence shows little variation in intensity need to

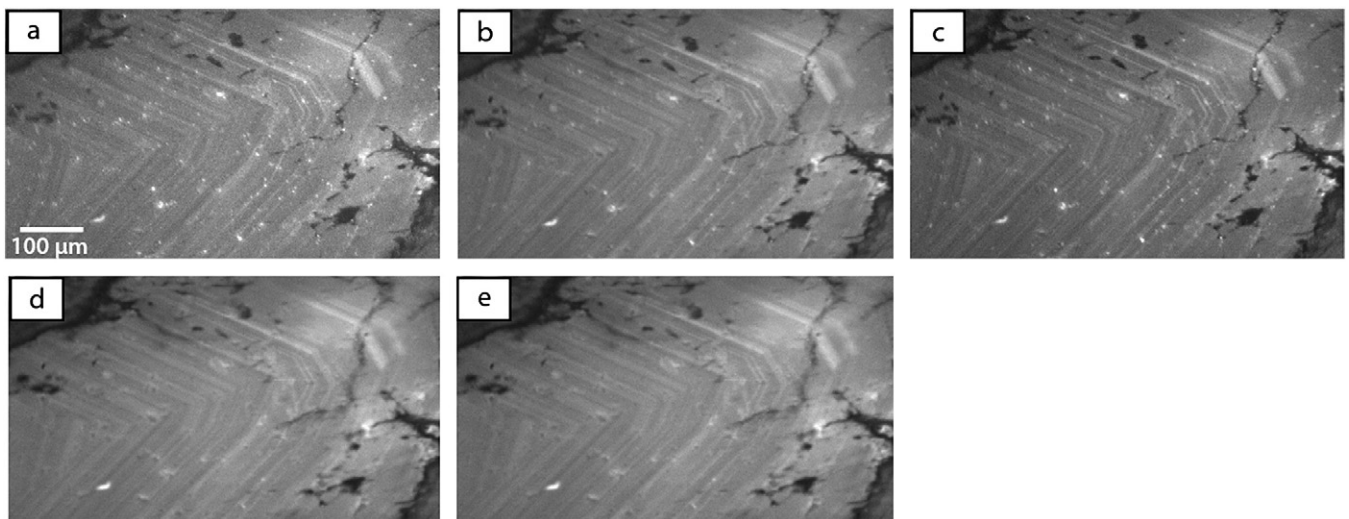


Fig. 6. High vacuum mode SEM-CL images of hydrothermal quartz from the Red Hills porphyry Mo–Cu deposit, Texas obtained using the XL30 ESEM beam spot size 6 (approximately 500 nm in diameter) and working distance 12 mm. a) 7.5 kV, HT – 655 V; b) 12 kV, HT – 605 V; c) 15 kV, HT – 570 V; d) 20 kV, HT – 535 V; and e) 30 kV, HT – 510 V. (HT = high tension photomultiplier tube voltage).

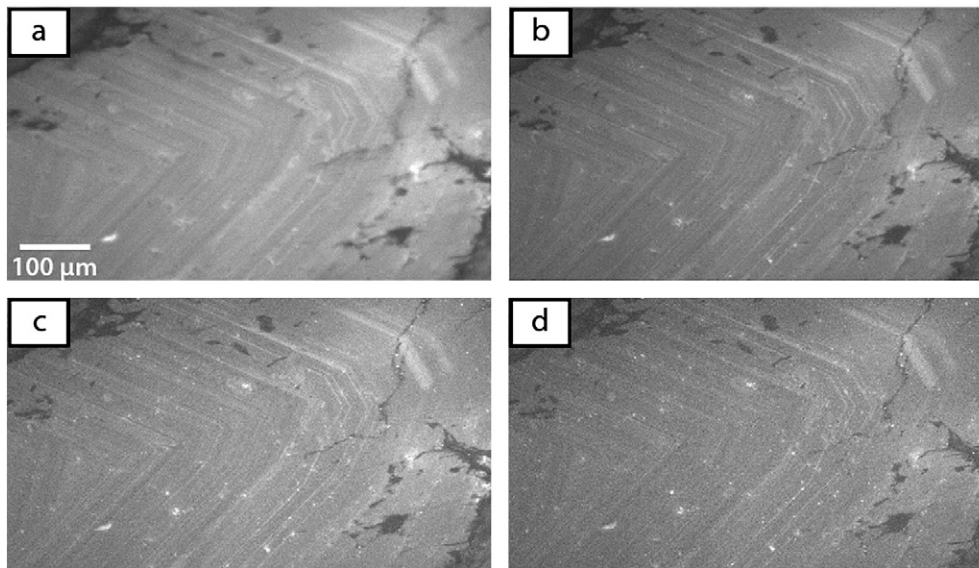


Fig. 7. Low vacuum mode SEM-CL images for the same area as imaged in Fig. 6, also using beam spot size 6 and working distance 12 mm. a) 12 kV, HT – 610 V; b) 15 kV, HT – 560 V; c) 20 kV, HT – 530 V; and d) 30 kV, HT – 530 V.

be imaged with a very high contrast setting; however, this procedure may produce grainy images and wash out the highly luminescent phases.

4.3.4. Color SEM-CL imaging

Color CL imaging requires the beam to scan over the same area three times using red, green, and blue optical filters. The red filter transmits light in the 595–850 nm range, the green filter in the 495–575 nm range, and the blue filter in the 185–510 nm range. The PMT voltage must be increased when scanning the sample with the red and green optical filters in order to generate adequate CL emissions. An increase of –150 V to –200 V is appropriate for the green filter and the red filter requires an increase of –200 V to –300 V. A “true-color” image is reconstructed from the separate RGB channels via an image processing program.

4.3.5. Image processing

Given the common situation that hydrothermal veins of interest typically have widths in the range of mm to cm, most SEM-CL studies involve the collection of multiple high resolution scans of smaller areas that then must be composited into a desired photomosaic. SEM-CL images are most useful when individual images are stitched into maps that reveal luminescence textures over multi-mm areas. Software available for SEM-CL imaging can automatically complete transects and compile images into a single seamless image that can be utilized without additional post-processing. It is also possible to obtain high quality seamless image compilations using one of the commercial or other photo stitching and merging applications to composite individual SEM-CL images into maps. For example, most CL images shown in this

review were produced using the photo merge function of Adobe® CS6. For these applications, the user should review appropriate instruction or tutorial offerings before beginning the image processing.

For all of these merging programs, the protocol for collecting the individual CL images is important, typically involving capture of a transect of overlapping images, with neighboring images containing an overlap of at least 40% of the area. For the highest quality final product, it is ideal to choose optimal working conditions with the first image and maintain the same conditions for all images captured. For these scans, the individual images can then be efficiently compiled into a single image. Most image-stitching software has an automated mode that aligns images without rotating or distorting the originals and merges the images into a seamless composition. Although these automated functions are rapid, they can result in poorly aligned photos and digital artifacts if the program does not automatically align the images properly. Thus, to ensure the most accurate cathodoluminescence maps, some manual alignment may be necessary to adjust improperly positioned images and blend the images to produce the desired result.

Merging SEM-CL mono-color images of the same field captured with RGB filters requires somewhat different procedures, but typically can be done using the same photo stitching and merging applications.

5. Application of quartz SEM-CL in hydrothermal ore deposits

Precipitation of metal sulfides in porphyry systems commonly occur in hydrothermal quartz veins. Extreme pressure buildup from exsolving fluids at the cupola of ascending magmatic stocks exceeds the yield strength of the overlying wall rock and eventually fractures the rock in a stockwork fashion. Hydrothermal fluids and porphyritic dikes then simultaneously propagate and ascend along these fractures, precipitating quartz and ore minerals at appropriate P–T conditions as the hot hydrothermal fluids cool. Various episodes of this style of hydrofracturing are common throughout the lifespan of a hydrothermal system. Thus, SEM-CL imaging is a useful tool to delineate sequential episodes of quartz precipitation and define the paragenetic sequences of hydrothermal vein sets.

5.1. Overview of hydrothermal systems using SEM-CL

Numerous researchers have applied SEM-CL imaging techniques to hydrothermal ore deposit studies, in particular, epithermal Au, porphyry Cu–Mo–Au and polymetallic skarn systems. Quartz CL shows a variety of

Table 1

Ideal photomultiplier tube voltages for specified accelerating voltages at high vacuum or low vacuum mode for SEM-CL imaging.

Mode	Accelerating voltage (kV)	PMT voltage (V)
High vacuum	7.5	–650 to –655
	12	–600 to –605
	15	–570 to –580
	20	–535 to –545
	30	–510 to –515
Low vacuum	12	–605 to –610
	15	–550 to –560
	20	–530 to –540
	30	–530 to –540

textures which are subdivided into primary growth features and a wide variety of secondary features, in part induced by post precipitation fracturing and dissolution (Figs. 8 and 9b). Secondary features are grouped into textures indicative of 1) local lower crystal order (increase of defect structures) and 2) local annealing (reduction of defect structures) (Rusk, 2012). SEM-CL complemented by fluid inclusion and trace element studies can provide T–P–X constraints to various fracturing and mineralization events from cross cutting vein sets as the hydrothermal fluids evolved (Boiron et al., 1992; Donovan et al., 2011; Müller et al., 2003b; Rusk and Reed, 2002; Rusk et al., 2008a,b; Wark and Watson, 2006).

According to Rusk (2012), hydrothermal quartz derived from specific ore deposit types display unique CL signatures that remain uniform over large areas. Porphyry systems contain quartz with well-preserved growth zones but typically show signs of dissolution and healed microfractures (Rusk, 2012). Epithermal systems display colloform textures, euhedral sector zoned crystals and very little dissolution textures. These textures are useful in sedimentary provenance studies when the geologic setting of the quartz is unknown especially during situations that involve stream or sediment sampling (Rusk, 2012).

Quartz SEM-CL petrography builds the framework for follow-up studies such as fluid inclusion microthermometry, hyperspectral CL mapping, stable isotope, and trace element mapping in specific quartz domains. Combination of quartz SEM-CL with these studies provides constraints on physiochemical conditions, rate of mineral precipitation, and compositional changes in fluid composition, which in turn can be applied to track variations in magmatic activity or to differentiate hydrothermal episodes of metal sulfide and quartz precipitation, or deformational or metamorphic events (Rusk, 2012; Tanner et al., 2013).

Since the development of Wark and Watson's (2006) TitaniQ geothermometer, trace element concentrations of Ti in individual crystals, measured by laser ablation inductively coupled plasma mass spectrometry or electron microprobe, have been utilized to assess the variations in temperature during crystal growth. When different generations of quartz are identified and their relative crystallization timing is

established by CL petrography, the heterogeneities in Ti concentration within individual grains in their specified domains may reflect large scale thermal histories and their spatial distribution of the hydrothermal system (Leeman et al., 2012). The Ti in quartz geothermometer, however, should only be applied in rutile-bearing phases where the thermodynamic activity of TiO₂ is in equilibrium (Zhao et al., 1999). Fluid inclusion analyses can be evaluated with respect to the specific quartz generations they are hosted in. Ideally, both the Ti in quartz thermometer and fluid inclusion microthermometry can be used to improve confidence in the thermal evolution of a hydrothermal system, as recorded in quartz precipitation.

Readily available samples of vein quartz from the Red Hills porphyry Mo–Cu deposit, Texas, USA, and the Ertsberg–Grasberg porphyry–skarn Cu–Au system, Indonesia, were used for SEM-CL imaging case studies following the guidelines mentioned above. The SEM-CL imaging of vein quartz followed thorough petrography, and provided more detailed textural information to identify different generations of quartz and any secondary fracture events.

5.2. Quartz SEM-CL of the Red Hills porphyry Mo–Cu deposit

5.2.1. Geologic setting, vein types and mineralization

The Red Hills porphyry Mo–Cu deposit is a Laramide age porphyry system located in Trans-Pecos, Texas, 8 km west of the Shafter silver mining district (Gilmer et al., 2003). The Red Hills is the easternmost known porphyry system in the North American Cordillera. The intrusive complex, composed of intermediate quartz monzonite porphyry, latite porphyry, quartz latite porphyry, and biotite porphyry, was emplaced into a Permian sedimentary sequence resulting in an extensive hornfels zone with local garnet skarn. Repeated episodes of stockwork fracturing throughout the intrusive complex allowed the transport and precipitation of Mo and Cu sulfides and quartz to form characteristic veins as the fluids cooled.

Correlating fracture and veining episodes with distinct alteration styles is difficult at the Red Hills due to the significant overprinting by phyllic alteration. Where present, potassic alteration is characterized by shredly biotite that is commonly altered to sericite. Chlorite–epidote propylitic alteration is generally barren of sulfides and forms above and lateral to the phyllic alteration zone. The argillic alteration zone and surficial leach cap contains supergene 2 mm to 1 inch alunite–kaolinite and jarosite veins with occasional vuggy quartz. Local zones of intense silicification also occur in Permian wallrocks and along faults.

Based on cross cutting relationships and Gustavson and Hunt's (1975) classification of porphyry vein styles, the vein types present at the Red Hills from oldest to youngest include: early barren quartz (EBQ) veins, sinuous quartz–molybdenite ± pyrite type A veins, planar quartz–molybdenite ± pyrite ± barite type B veins, pyrite ± quartz ± pyrrhotite ± chalcocopyrite ± chalcocite ± bornite type C veins, sinuous quartz ± pyrite type Da veins, and quartz–pyrite ± chalcocopyrite ± sphalerite type Db veins. Detailed descriptions of the vein types are located in Table 2. Hypogene mineralization of molybdenite (60.2 ± 0.3 Ma) is primarily hosted along the margins or centerlined in types A and B quartz-rich veins, but can also be found disseminated within the host rock. Chalcocopyrite is typically found as inclusions with pyrrhotite and chalcocite within pyrite in type C veins, rarely in type D veins, or as disseminations.

5.2.2. SEM-CL textures of the hydrothermal vein quartz and their implications

SEM-CL imaging of the vein quartz from each vein type of the Red Hills porphyry Mo–Cu deposit provides an opportunity to study textural differences between quartz generations associated with each vein type. In conjunction with trace element studies, these vein quartz textures may delineate the relationships between discrete quartz and metal sulfide generations associated with different magmatic and hydrothermal

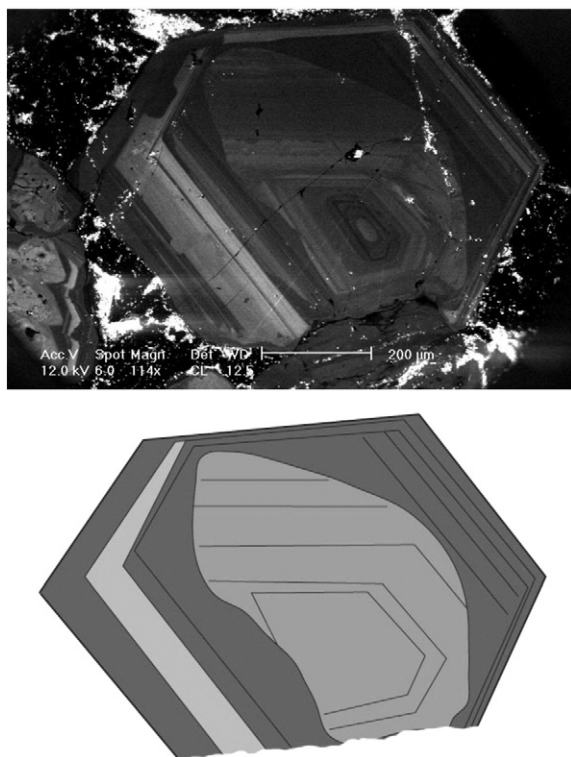


Fig. 8. Dissolution-modified well-zoned early quartz core overgrown by well-zoned quartz from early Kali stockwork, Ertsberg–Grasberg District, Indonesia. From Baline (2007).

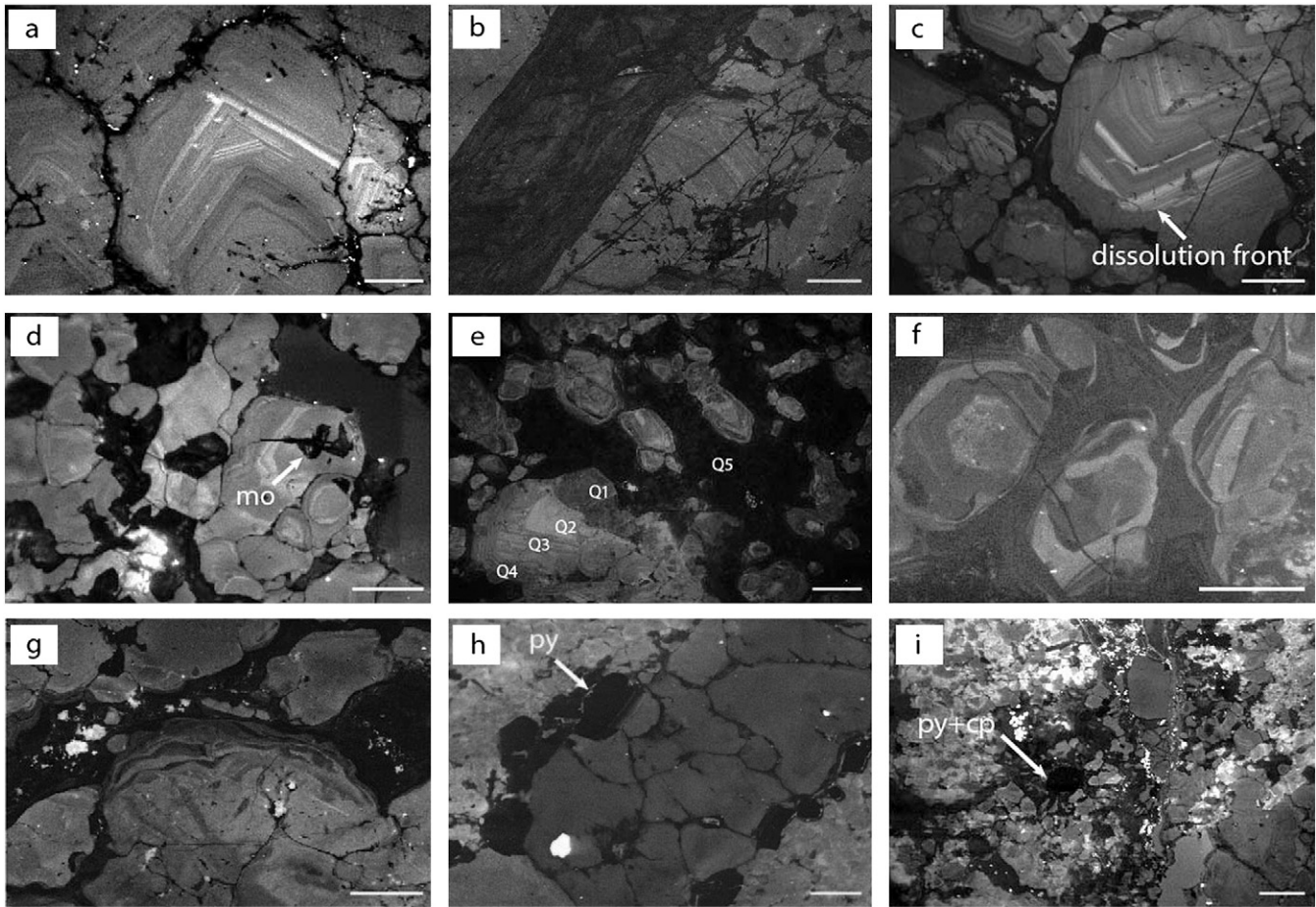


Fig. 9. Vein quartz from the Red Hills displays a myriad of complex textures illuminated by SEM-CL. The following are characteristic textures found within the various quartz-bearing veins: a) Type A vein: Mosaics of euhedrally zoned, inward oriented quartz which indicates quartz growth began in open space fractures. b) Type B vein: Splatter and cobweb texture of microfractures cutting euhedrally zoned quartz cut by a CL-dark band (healed fracture). These dark microfractures correspond to trails of secondary fluid inclusions. c) Type Da vein: Euhedrally zoned quartz with oscillating zones of CL-intensities and thickness of a type Da vein. Euhedral quartz that has been partially dissolved and overgrown by homogenous, gray-CL quartz. d) Type A vein: Mosaic of fine grained, CL-bright equant quartz grains with internal wavy growth zonations. Dark CL quartz is observed in areas of molybdenite deposition, typically along grain boundaries but occasionally within intergranular fractures in quartz. e) Microbreccia texture demonstrating the superposition of multiple hydrothermal events of different quartz generations. Q1 is igneous quartz overgrown by CL-bright mosaic quartz of Q2 which is dissolved and overgrown by CL-darker quartz of Q3. Q3 displays wavy concentric banding which is dissolved and overgrown by Q4 euhedral quartz with faint CL bands. CL-bright cores with CL-darker overgrowths by dissolution are possibly caused by fluid cooling through the zone of retrograde quartz solubility. All of these quartz generations are then fractured by late CL-dark fractures Q5. f) Quartz with internal wavy growth zonation dissolved and overgrown by dark-CL quartz. g) Wavy concentric banding (WCB) quartz with dark-CL quartz within fractures. WCB has been attributed to post-crystallization elemental diffusion. h) Homogenous quartz grains within a type Da vein. Pyrite is deposited along the margins of the vein. i) Pyrite with chalcopyrite inclusions associated with dull-homogenous-CL quartz and coarse grained sericite occurs as fractures that cut through wallrock. Early CL-bright quartz cut by later CL-darker quartz with euhedral growth zones, cut by CL-dark fractures. The white scale bar represents 100 μm . mo = molybdenite, py = pyrite, cp = chalcopyrite, and Q1–Q5 = quartz 1 through quartz 5.

pulses to understand the variations of the P–T–X conditions of hydrothermal system at the Red Hills.

Preliminary SEM-CL petrography of the vein quartz at the Red Hills revealed complex textures for each vein type (Table 3). Many veins contain multiple quartz generations where some experienced dissolution and fracturing. The EBQ quartz displays homogenous, dull CL textures, which is likely due to recrystallization from later stage fracture and veining events. The type A qz–mo veins reveal first generation molybdenite precipitated along grain boundaries in bright to moderate CL quartz (Figs. 9a, d and 10). Fig. 10 shows a SEM-CL photomosaic of an early, asymmetric quartz–molybdenite \pm pyrite type A vein. Near the margins of the vein and rarely along the vein center, molybdenite is present along the grain boundaries of fine grained, equant quartz which characteristically displays internal wavy growth zonations. This layer acted as a substrate for euhedral, inward oriented quartz to grow on and into open space. The euhedral quartz crystals typically display thin concentric growth zones of varying CL intensities ranging from 5 to 50 μm in thickness. Wavy concentric banding (WCB) is typically observed near the tips of euhedral quartz which experienced grain boundary migration upon vein

closure. Late stage fracturing is evident by thin, dark CL microfractures that cut through the entire vein and correspond to secondary trails of fluid inclusions.

Trace element mapping of euhedral quartz in type A veins indicates that the CL intensities reflect variations of Ti concentrations within individual growth zones (Fig. 10). Bright-CL growth zones of euhedral quartz correlate with higher Ti concentrations and dark CL zones are depleted in Ti compared to CL-bright zones. Thus, light bands of higher CL intensity contain elevated Ti, whereas darker CL bands contain lower concentrations.

Type B qz–mo–py veins reveal thin, oscillatory zoning of inward oriented quartz crystals that precipitated into open space. Second generation molybdenite is deposited along the vein margins similar to type A veins, but pyrite occupies the center of the vein. Abundant late stage, healed fractures and microfractures (splatter and cobweb textures = SC) postdate the formation of type B veins (Fig. 9b). Healed fractures contain dark-CL quartz which appear either euhedral or banded in shape. Sphalerite, barite, calcite, anhydrite, and silver-bearing phases were deposited relatively late in the system within the interstices of types A and B veins.

Table 2
Vein description chart for the characteristic veins at the Red Hills porphyry Mo–Cu deposit, Texas, USA.

Early to Late	Vein type		Description
	Supergene	Hematite/Goethite	
Alunite		Crystalline yellow-brown alunite in planar, vuggy vein up to 1 cm wide found only in the leach cap and argillic alteration zone.	
White Alunite		Very fine grained, microcrystalline alunite veins ranging from 1mm up to 2cm wide veins which are found in the leach cap but can extend up to 200 ft deeper than the base of the oxide zone.	
Hypogene	C		Pyrite±quartz±pyrrhotite±chalcopyrite±chalcocite with sericite halo. Discontinuous deposition of pyrite within quartz veinlet. Pyrite may occupy up to 98% of the vein. If found within veins, Cu deposition is primarily constrained to C- and D-type veins and rarely Ba veins. Pyrrhotite, chalcopyrite, and digenite are typically inclusions within pyrite. Chalcopyrite inclusions within pyrite is often associated with pyrrhotite grains that surround the chalcopyrite but can be found as isolated inclusions. Chalcocite occurs as small, isolated inclusions within pyrite as well and commonly coats fractures and voids within pyrite grains. Chalcopyrite also occurs as small disseminations within quartz-sericite matrix and commonly contains chalcocite rims.
	D	Db	Quartz-pyrite±chalcopyrite±sphalerite with fine grained, sericite halo.
		Da	Sinuuous quartz±pyrite without alteration halos.
	B	Ba	Euhedral quartz-molybdenite±pyrite±pyrrhotite±chalcopyrite±chalcocite (rare). Molybdenite is typically disseminated and deposited along vein margins in between quartz grain boundaries or within fractures. Pyrite fills in the center of the vein. Chalcopyrite is commonly associated with pyrrhotite and is encompassed in the pyrrhotite which exists as small inclusions within pyrite. This vein is likely a result of a B vein overprinted by a C vein.
		B	Euhedral quartz-molybdenite±pyrite±barite. Planar with internal parallel banding qz-mo deposition with no alteration halos. Mo typically deposited along vein margins and pyrite fills in the center line of the vein.
	A		Sinuuous quartz quartz-molybdenite±pyrite veins or veinlets.
	EBQ		Early barren quartz, typically sinuous.

Table 3
SEM-CL characteristics of vein quartz from specific vein types at the Red Hills. Q = quartz, py = pyrite, po = pyrrhotite, cp = chalcopyrite, cc = chalcocite, mo = molybdenite, OGZ = oscillatory growth zones, BCDO = CL bright cores with CL darker overgrowths, IWGZ = internal wavy growth zones, SC = splatter and cobweb, and WCB = wavy concentric banding.

Early to Late	Vein	Mineral	Morphology	CL Intensity	CL Textures	
		C	Q1	Euhedral to equant	Moderate - Low	OGZ, BCDO, IWGZ, Dissolution
Py±po±cp±cc			Anhedral, bleb	NA		
D		Db	Q1	Anhedral	Bright	IWGZ, BCDO
			Q2	Anhedral	Low	IWGZ
			Pyrite	Anhedral, bleb	NA	
		Sericite	Euhedral	NA		
		Da	Q1	Euhedral	Moderate – High	OGZ, Dissolution, SC
Py			Bleb	NA		
B		Mo	Euhedral	NA		
		Q1	Equant	Moderate	Mosaic, IWGZ	
		Q2	Euhedral	Moderate - High	Mosaic, OGZ, Dissolution,	
		Q3	Equant	Moderate -Low	IWGZ, CGZ, DE, Dissolution,	
		Py	Anhedral	NA		
		Q4	Euhedral	Low	OGZ	
A		Mo	Euhedral	NA	NA	
		Q1	Equant	High - Moderate	Mosaic, IWGZ, BCDO	
		Q2	Euhedral	High -Moderate	Mosaic, OGZ, TB, Dissolution	
		Q3	Curvilinear – Secondary Growth	Moderate – Low	CGZ, SC, BCDO, SC	
EBQ	Q1	Bleb	Moderate	WCB, homogenous		
	Q2	Linear	Low	SC		

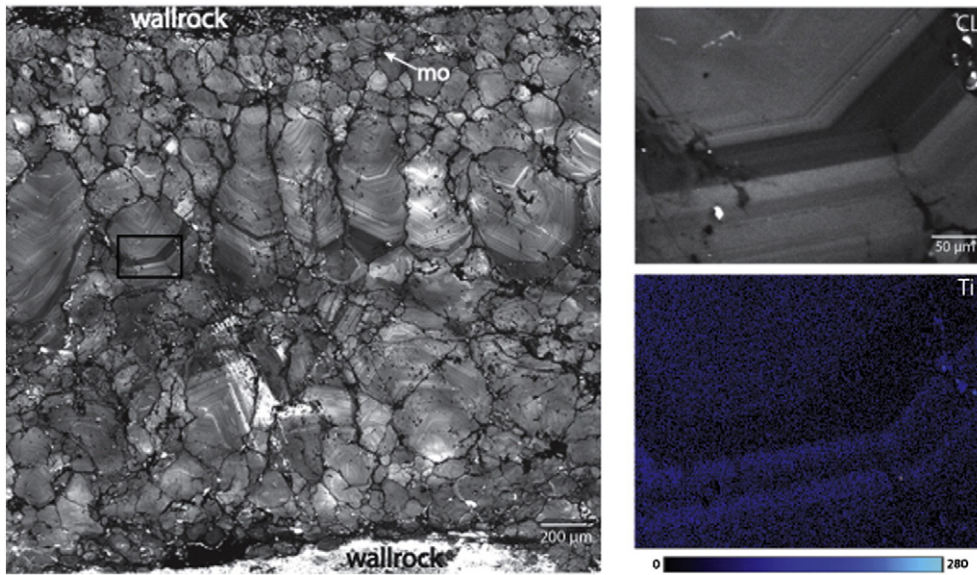


Fig. 10. Left: Composite panchromatic SEM-CL images of a quartz-molybdenite vein from the Red Hills. Quartz along the vein margins are fine grained, hypidiomorphic mosaics with irregular growth zones that contain molybdenite deposited along grain boundaries. Large euhedral quartz grows after the fine grained quartz and displays sector zoning of variable CL intensities. The black box is the location where the WDS X-ray mapping of trace element was performed. Top right: SEM-CL image at greater magnification of the area highlighted in black box on the left figure. Strong variations of CL intensity within individual growth zones of variable thickness are apparent. Secondary microfractures at the right and left bottom corners are also apparent. Bottom right: Ti WDS map shows strong positive correlation with CL bright growth zones compared to CL dark growth zones which contain lower concentrations of Ti. Blue scale bar represents the Ti concentration. mo = molybdenite.

Vein quartz textures in type D veins display the greatest complexity in crystal growth (Fig. 9e, g, h and f). For example, five different quartz precipitation events are evident in one sample, with irregular, turbid growth zoning of early quartz, followed by the overgrowth of bright CL quartz mantles following a dissolution event (Fig. 9e). A third generation of concentric to wavy growth zones of alternating light and dark CL bands mimics the shape of the embayments of the bright CL quartz. A major dissolution event most likely caused by retrograde quartz solubility as the fluids cooled followed the third quartz precipitation event. The fourth quartz precipitation event is defined by thinner concentric bands of darker gray CL emission. A final dilational fracturing dislodged and comminuted earlier quartz. This dilational event allowed the final flux of hydrothermal fluids to permeate within the fractures and precipitate the last episode of interlocking, euhedral, dark-CL quartz cement. In samples which contained euhedral quartz in type Da veins, higher Ti concentrations showed positive correlations with CL-bright growth zones and Al weakly correlated to bright CL zones. Dark CL quartz cement could not be correlated with trace element abundance, as concentrations were below EPMA detection limits.

The SEM-CL textures of vein quartz reveal a complex fracturing and vein-filling history for the Red Hills hydrothermal system. Preliminary trace element studies indicate that the bright CL growth zones in all vein quartz correlate with higher Ti concentrations and rarely with Al. These correlations may assist in identifying fluid inclusion assemblages within the specified growth zones to constrain the P–T–X evolution of the hydrothermal fluids responsible for the formation of the Red Hills deposit.

5.3. Quartz SEM-CL of Ertzberg–Grasberg porphyry–skarn Cu–Au system

5.3.1. Geologic setting and mineralization events

The Ertzberg–Grasberg District is a 50 km² region of world class Cu–Au porphyry and Cu–Au skarn deposits in the highlands of Papua, Indonesia. The district is subdivided into the Grasberg Intrusive Complex and the Ertzberg Intrusive Complex, each of which is centered on a dioritic intrusion. Cu–Au mineralization throughout the district is believed to have occurred between 3.3 and 2.5 Ma by genetically related

fluid derived from a common magmatic source (Leys et al., 2012). Luminescence textures in vein quartz from the Ertzberg Intrusive Complex and the Grasberg Igneous Complex provide an opportunity to compare quartz textures in giant ore deposits that are spatially, temporally and genetically related.

5.3.2. SEM-CL textures of the quartz and their implications

Penniston-Dorland (1997a,b, 2001) first described quartz zonation patterns revealed by SEM-CL of quartz-sulfide veining in the upper part of the Grasberg Igneous Complex. Baline (2007) used SEM-CL techniques to characterize the relationship between trace element composition and luminescence textures in vein quartz associated with Cu–Au mineralization in the Deep Grasberg ore zone, and identified fluid inclusion populations restricted to specific growth zones in vein quartz. Reconnaissance SEM-CL studies of quartz veins in the Ertzberg Igneous Complex revealed textures similar to those found in the Grasberg Igneous Complex.

The SEM-CL images revealed a variety of textures consistent with the classifications used by Penniston-Dorland (2001) and Baline (2007) for describing quartz veins in the Grasberg Igneous Complex (Table 4 and Figs. 2, 8 and 11). Euhedral concentric zoning in quartz delineates parallel to sub-parallel bands of uniform CL intensity that emanate outward from the point at which the crystal nucleation occurred. In Fig. 11, these bands are well defined in highly luminescent quartz crystals (qz₁) that grow inward from the selvage. Couplets are light to dark euhedral, concentric zoning pairs in the younging direction of crystal growth (Baline, 2007). Truncated zoning refers to concentric zones that abruptly stop at the interface of different orientations of concentric zoning, which propagates outwards in the direction of crystal growth. Late stage low luminescence quartz is commonly in contact with anhydrite or sulfides. Brittle deformation structures are typically healed with micro-fractured quartz (qz₂) which emits low intensity luminescence and commonly cross cuts qz₁. Dissolution structures in quartz manifest where anhedral quartz of varying luminescence fills veins that have irregular edges. This texture is indicative of dissolution, which is supported by the truncation of earlier concentric zonations. Irregular turbulent zones and fluid inclusions have not been observed

Table 4

Features and relative timing of quartz vein mineralization events in the Deep Mill Level Zone (DMLZ). From Baline (2007) and Penniston-Dorland (2001).

Mineral	Relative CL Intensity	Morphology	Textures	Stage			
				I	II	III	IV
Quartz 1	Moderate - High	Euhedral	Concentric Growth Zonation, Couplets, Pinched Out, Undulatory, Microfractures, Dissolution	_____			
Quartz 2	Very Low	Linear - Bleb	Microfractures and Brittle Deformation		_____		
Quartz 3	Low	Curvilinear - Secondary Growth	Darkened Edge, Concentric Growth Zonation, Dissolution			_____	
Anhydrite	Very High	Subhedral - Anhedral - Curvilinear					_____
Pyrite/Chalcopyrite	None	Euhedral - Anhedral					_____

with scanned cathodoluminescence imaging in the Ertsberg Intrusive Complex samples studied.

The above SEM-CL textures were used to identify three distinct mineralization events during quartz–anhydrite–sulfide vein growth in the Ertsberg Igneous Complex (Table 5). Early, highly luminescent quartz (qz_1) forms concentrically veined crystals that broaden as they grow into open space and overtake smaller crystals (Penniston-Dorland, 2001). These textures predate at least one brittle deformation event, as evidenced by qz_2 sealed micro-fractures crosscutting qz_1 . Rusk and Reed (2002) described similar fractures with notable offset in the Butte porphyry copper deposit, which they deduced to be the micro-structural expression of large scale faulting. However, in the Ertsberg diorite, the qz_2 -sealed fractures do not record offset at the time of qz_2 formation, so the mechanical closure of open quartz fractures may be a more plausible mechanism for micro-fracture formation than faulting. Lastly, late anhydrite–pyrite–chalcopyrite mineralization fills open spaces in the vein. In other porphyries like the Butte porphyry, the sequence of highly luminescent quartz deposition is followed by a dissolution event and low luminescence quartz deposition, which is consistent with quartz solubility changes resulting from isothermal pressure drop (at greater than 500 °C) followed by isobaric cooling (Reed and Rusk, 2002).

As demonstrated by Baline (2007), the concentric zones revealed by SEM-CL imaging can be used as guidelines for identifying fluid inclusion

populations within quartz crystals (Fig. 11). If multiple-populations of intact primary inclusions are identified within a crystal or neighboring crystals, it is conceivable to deduce the temporal evolution of P–T–X condition during crystallization based on correlation with quartz textures revealed by SEM-CL. In addition, trace element analysis of the distinct quartz precipitation episodes makes it possible to define the features of hydrothermal veining episodes in the Ertsberg East Skarn and compare them with the features for the quartz veins in the Grasberg Igneous Complex (Baline, 2007; Penniston-Dorland, 1997a,b, 2001). Furthermore, the quartz generations revealed by SEM-CL may be correlated between mineral deposits within a district, to reveal the fundamental characteristics of ore-stage quartz veining.

6. Summary

SEM-CL is an ideal technique for imaging hydrothermal quartz from porphyry and epithermal systems because it is able to reveal complex growth, dissolution, and fracturing textures which are not visible by other methods. Unique CL responses elucidate the geological environment and thus help understand the provenance of an unknown sample, particularly for soil or sediment samples. When integrated with other analytical techniques such as fluid inclusion microthermometry, trace element analysis, and hyperspectral mapping, quartz SEM-CL imaging can unveil complex growth and fracture histories of an ore deposit system. This study shows that obtaining high quality SEM-CL panochromatic or monochromatic images is highly dependent on sample preparation and optimized experimental conditions. The SEM-CL experimental conditions discussed in this study produced high quality images that clearly reveal complex textures of the vein quartz from typical porphyry–skarn ore systems.

Acknowledgments

Insightful discussions with Dr. Andras Fall and Dr. Peter Eichhubl related to sample degradation of fluid inclusions caused by SEM-CL are greatly appreciated. Also, thanks to Dr. Nathan Miller for information regarding the degree of sample destruction caused by LA-ICPMS studies. Research in the Ertsberg–Grasberg District has been supported by PT Freeport Indonesia. Studies on the Red Hills deposit were made possible by the financial support provided by the University of Texas' Jackson School of Geosciences, the Society of Economic Geologists, and the West Texas Geological Society.

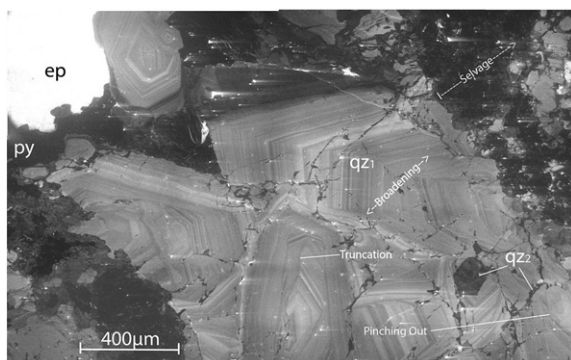


Fig. 11. Composite SEM-CL image of a qz – an – py – cp vein from the Ertsberg Diorite. This image displays several of the textures used to define quartz veining in the Grasberg Igneous Complex and illustrates the crosscutting relationships elucidated by SEM-CL in the Ertsberg–Grasberg District (Baline, 2007; Penniston-Dorland, 2001). Symbols: qz_1 = early concentrically zoned quartz; qz_2 = dark quartz in healed fractures; ep = epoxy; py = pyrite.

Table 5
Quartz vein textures in the DMLZ. All samples demonstrate concentric growth, microfractures, dissolution, irregular turbulence, and darkened edges. However, irregular turbulence was not identified in the DMLZ samples. More data are necessary, but there does not appear to be any correlation between textures and sample location or between textures and lithology. After Baline (2007).

Sample ID	Unit	Vein thickness (cm)	Concentric growth zonation	Average # of couplets	Pinched out	Truncated	Undulatory	Micro-fractures	Dissolution	Irregular turbulence	Darkened edges
TE01-16-310.0	Te diorite, anh + py vein	0.6	x	3	x	x		x	x		x
TE01-16-585.2	Te diorite, anh + qtz vein	1.2	x	3				x	x		x
TE01-16-748.7	Kkel hornfels	0.5	x	2		x		x	x		x
TE01-16-870.4	Kkel hornfels	0.8	x	6		x	x	x	x		x

References

- Bahadur, H., 1993. Hydroxyl defects and electrodiffusion (sweeping) in natural quartz crystals. *J. Appl. Phys.* 73, 7790–7797.
- Baline, L.M., 2007. Hydrothermal fluids and Cu–Au mineralization of the Deep Grasberg Porphyry Deposit, Papua, Indonesia. University of Texas at Austin.
- Bernet, M., Bassett, K., 2005. Provenance analysis by single-quartz-grain SEM-CL/optical microscopy. *J. Sediment. Res.* 75, 492–500.
- Boggs, S.J., Kwon, Y.-I., Goles, G.G., Rusk, B.G., Krinsley, D., Seyedolali, A., 2002. Is quartz cathodoluminescence color a reliable provenance tool? A quantitative examination. *J. Sediment. Res.* 72, 408–415.
- Boiron, M.C., Essarraj, S., Lespinnasse, M., Poty, B., 1992. Identification of fluid inclusions in relation to their host microstructural domains in quartz by cathodoluminescence. *Geochim. Cosmochim. Acta* 56, 175–185.
- Crookes, W., 1879. Contributions to molecular physics in high vacua. *Philos. Trans. R. Soc. Lond.* 641–662.
- Dennen, W., 1965. Stoichiometric substitution in natural quartz. *Geochim. Cosmochim. Acta* 30, 1235–1241.
- Donovan, J.J., Lowers, H.A., Rusk, B.G., 2011. Improved electron probe microanalysis of trace elements in quartz. *Am. Mineral.* 96, 274–282.
- Flem, B., Larsen, R.B., Grimstvedt, A., Mansfeld, J., 2002. In situ analysis of trace elements in quartz by using laser ablation inductively coupled plasma mass spectrometry. *Chem. Geol.* 182, 237–247.
- Gilmer, A.K., Kyle, J.R., Connelly, J.N., Mathur, R.D., Henry, C.D., 2003. Extension of laramide magmatism in southwestern North America into Trans-Pecos Texas. *Geology* 31, 447.
- Götze, T., Pettke, T., Ramseyer, K., Koch-Muller, M., Mullis, J., 2011. Cathodoluminescence properties and trace element signature of hydrothermal quartz: a fingerprint of growth dynamics. *Am. Mineral.* 96, 802–813.
- Götze, J., 2009. Chemistry, textures and physical properties of quartz—geological interpretation and technical application. *Mineral. Mag.* 73, 645–671.
- Götze, J., Freiberg, T.U.B., 2012. Application of cathodoluminescence microscopy and spectroscopy in geosciences. *Microsc. Microanal.* 18, 1270–1284.
- Götze, J., Plötze, M., Habermann, D., 2001. Origin, spectral characteristics and practical applications of the cathodoluminescence of quartz—a review. *Mineral. Petrol.* 225–250.
- Gustavson, L.B., Hunt, J.P., 1975. The porphyry copper deposit at El Salvador, Chile. *Econ. Geol.* 70, 857–912.
- Hamers, M.F., Drury, M.R., 2011. Scanning electron microscope–cathodoluminescence (SEM-CL) imaging of planar deformation features and tectonic deformation lamellae in quartz. *Meteorit. Planet. Sci.* 46, 1814–1831.
- Henry, D., 2012. Cathodoluminescence theory [WWW Document] URL http://serc.carleton.edu/research_education/geochemsheets/CLTheory.html (accessed 3.25.14).
- Landtwinig, M.R., Pettke, T., 2005. Relationships between SEM–cathodoluminescence response and trace-element composition of hydrothermal vein quartz. *Am. Mineral.* 90, 122–131.
- Leeman, W.P., MacRae, C.M., Wilson, N.C., Torpy, A., Lee, C.-T.A., Student, J.J., Thomas, J.B., Vicenzi, E.P., 2012. A study of cathodoluminescence and trace element compositional zoning in natural quartz from volcanic rocks: mapping titanium content in quartz. *Microsc. Microanal.* 18, 1322–1341.
- Lehmann, G., 1975. On the colour centers of iron in amethyst and synthetic quartz: a discussion. *Am. Mineral.* 60, 335–337.
- Lehmann, K., Berger, A., Götze, T., Ramseyer, K., Wiedenbeck, M., 2009. Growth related zonations in authigenic and hydrothermal quartz characterized by SIMS-, EPMA-, SEM-CL- and SEM-CC-imaging. *Mineral. Mag.* 73, 633–643.
- Leys, C.A., Cloos, M., New, B.T.E., MacDonald, G.D., 2012. Copper–gold +/- molybdenum deposits of the Ertsberg–Grasberg District, Papua, Indonesia. *Econ. Geol. Spec. Publ.* 16, 215–235.
- Machel, H., Burton, E., 1991. Factors governing cathodoluminescence in calcite and dolomite, and their implications for studies of carbonate diagenesis. In: CE, B., OC, K. (Eds.), *Luminescence Microscopy and Spectroscopy: Qualitative and Quantitative Applications*. SEPM Short Course, Tulsa, pp. 37–57.
- Marshall, D.J., 1988. Cathodoluminescence of Geological Materials. Unwin Hyman, Boston.
- Matter, A., Ramseyer, K., 1985. Cathodoluminescence microscopy as a tool for sedimentary provenance studies of sandstones. NATO ASI Series C on Provenance of Arenites. D. Reidel Publishing Company, Dordrecht-Boston, pp. 191–211 (International).
- Muller, A., Kronz, A., Breiter, K., 2002. Trace elements and growth patterns in quartz: a fingerprint of the evolution of the subvolcanic Podlesí Granite System (Krušné hory Mts., Czech Republic). *Bull. Czech Geol. Surv.* 77, 135–145.
- Müller, A., René, M., Behr, H.-J., Kronz, A., 2003a. Trace elements and cathodoluminescence of igneous quartz in topaz granites from the Hub Stock. *Mineral. Petrol.* 79, 167–191.
- Müller, A., Wiedenbeck, M., van den Kerkhof, A.M., Kronz, A., Simon, K., 2003b. Trace elements in quartz—a combined electron microprobe, secondary ion mass spectrometry, laser-ablation ICP-MS, and cathodoluminescence study. *Eur. J. Mineral.* 15, 747–763.
- Owen, M.R., Carozzi, A.V., 1986. Southern provenance of upper Jackfork Sandstone, southern Ouachita Mountains: cathodoluminescence petrology. *Geol. Soc. Am. Bull.* 97, 110–115.
- Pagel, M., Barbin, V., Blanc, P., Ohnenstetter, D., 2000. Cathodoluminescence in Geoscience. Springer, Berlin, Heidelberg, New York.
- Penniston-Dorland, S.C., 1997a. Veins and alteration envelopes in the Grasberg Igneous Complex, Gunung Bijih (Ertserg) District, Irian Jaya, Indonesia. M.S. thesis The University of Texas, Austin (at).
- Penniston-Dorland, S.C., 1997b. Scanned cathodoluminescence of quartz and interpretation of textures in quartz-sulfide veins in the Grasberg Igneous Complex, a porphyry copper deposit. *Geol. Soc. Am. Abstr.* A-61.
- Penniston-Dorland, S.C., 2001. Illumination of vein quartz textures in a porphyry copper ore deposit using scanned cathodoluminescence: Grasberg Igneous Complex, Irian Jaya, Indonesia. *Am. Mineral.* 86, 652–666.
- Rusk, B.G., 2012. Cathodoluminescence and trace elements in hydrothermal quartz. In: Götze, J., Möckel, R. (Eds.), *Quartz: Deposits, Mineralogy and Analytics*. Springer, Berlin, pp. 307–329.
- Rusk, B., Reed, M., 2002. Scanning electron microscope–cathodoluminescence analysis of quartz reveals complex growth histories in veins from the Butte porphyry copper deposit, Montana. *Geology* 30, 727–730.
- Rusk, B.G., Lowers, H.A., Reed, M.H., 2008a. Trace elements in hydrothermal quartz: relationships to cathodoluminescent textures and insights into vein formation. *Geology* 36, 547.
- Rusk, Brian G., Reed, Mark H., Dilles, J.H., 2008b. Fluid inclusion evidence for magmatic-hydrothermal fluid evolution in the porphyry copper–molybdenum deposit at Butte, Montana. *Econ. Geol.* 103, 307–334.
- Seyedolali, A., Krinsley, D.H., Boggs Jr., S., O'Hara, P.F., Dypvik, H., Goles, G.G., 1997. Provenance interpretation of quartz by scanning electron microscope–cathodoluminescence fabric analysis. *Geology* 25, 787–790.
- Sippel, R.F., 1968. Sandstone petrology, evidence from luminescence petrography. *J. Sediment. Res.* 38, 530–554.
- Spear, F.S., Wark, D.A., 2009. Cathodoluminescence imaging and titanium thermometry in metamorphic quartz. *J. Metamorph. Geol.* 27, 187–205.
- Sprunt, E.S., Dengler, L.A., Sloan, D., 1978. Effects of metamorphism on quartz cathodoluminescence. *Geology* 6, 305.
- Tanner, D., Henley, R.W., Mavrogenes, J.A., Holden, P., 2013. Combining in situ isotopic, trace element and textural analyses of quartz from four magmatic-hydrothermal ore deposits. *Contrib. Mineral. Petrol.* 166, 1119–1142.
- Van den Kerkhof, A.M., Kronz, A., Simon, K., Scherer, T., 2004. Fluid-controlled quartz recovery in granulite as revealed by cathodoluminescence and trace element analysis (Bamble sector, Norway). *Contrib. Mineral. Petrol.* 146, 637–652.
- Vasyukova, O., Goemann, K., Kamentetsky, V.S., MacRae, C.M., Wilson, N.C., 2013a. Cathodoluminescence properties of quartz eyes from porphyry-type deposits: implications for the origin of quartz. *Am. Mineral.* 98, 98–109.
- Vasyukova, O., Kamentetsky, V.S., Goemann, K., Davidson, P., 2013b. Diversity of primary CL textures in quartz from porphyry environments: implication for origin of quartz eyes. *Contrib. Mineral. Petrol.* 166, 1253–1268.
- Wark, D.A., Watson, E.B., 2006. TitanQ: a titanium-in-quartz geothermometer. *Contrib. Mineral. Petrol.* 152, 743–754.
- Weil, J., 1984. A review of electron spin spectroscopy and its application to the study of paramagnetic defects in crystalline quartz. *Phys. Chem. Miner.* 10, 149–165.
- Xu, G., 2012. Fluid inclusion studies of microfractures in Eriboll Formation, NW Scotland: insights into timing of fracture opening. M.S. thesis University of Texas, Austin (at).
- Zhao, D., Essene, E.J., Zhang, Y., 1999. An oxygen barometer for rutile–ilmenite assemblages: oxidation state of metasomatic agents in the mantle. *Earth Planet. Sci. Lett.* 166, 127–137.
- Zinkernagle, U., 1978. Cathodoluminescence of quartz and its application to sandstone petrology. *Contrib. Sedimentol.* 8, 1–69.